Title

Analytic Prediction of Rotor Broadband Noise with Serrated Trailing Edges with Applications to Urban Air Mobility Aircraft

Journal

Journal of the American Helicopter Society, 69(3)

ISSN

0002-8711

Authors

Li, Sicheng Kevin
Lee, Seongkyu

Publication Date

2024-07-01

DOI

10.4050/jahs.69.032005

Peer reviewed

Analytic Prediction of Rotor Broadband Noise with Serrated Trailing Edges with Applications to Urban Air Mobility Aircraft

Sicheng Kevin Li
Assistant Professor,
University of Hartford,
West Hartford, Connecticut, 06117

Seongkyu Lee
Professor,
University of California,
Davis, California, 95616

Abstract

Theoretical predictions for broadband noise generated by rotors with serrated trailing edges are presented. This study extends Lyu and Ayton's model for serrated trailing-edge noise to account for factors such as finite span length, the accurate acoustic attenuation rate of trailing-edge noise, modified spanwise wavenumber, and the proper scattering factor. This new model is implemented in the rotorcraft broadband noise tool, UCD-QuietFly. The validation results demonstrate a satisfactory level of agreement with the experimental data for serrated trailing-edge noise of a wing section, a hovering rotor, and a forward-flight rotor. Next, the effects of serration parameters, such as the number of serrations, serrations' starting radial location, serration geometry, and serration height, on rotor broadband noise are investigated. For example, it is observed that sine-wave, chopped peak, or saw-tooth serration shapes provide the most significant noise reduction among the various shapes

Presented at the Vertical Flight Society 78th Annual Forum & Technology Display, Fort Worth, Texas, USA, May 10-12, 2022.

considered. Finally, broadband noise reduction through serrations is applied to two urban air mobility aircraft scenarios: a 6-passenger quadrotor and a quiet helicopter. For the quadrotor, serrated trailing edges show a noise reduction potential of over 9 dB, with higher reductions observed at higher tip speeds and fewer blades. A quiet helicopter equipped with serrated blades in forward flight achieves a maximum noise reduction of over 10 dB in the forward direction.

Nomenclature

c	chord length, m
c_0	speed of sound, m/s
E_n	serration shape coefficient
f	frequency, Hz
$F(\eta)$	serration geometry function
$2h$	serration height, m
k	acoustic wavenumber, ω/c_0
k_x	aerodynamic wavenumber, ω/V_c, 1/m
k_y	spanwise wavenumber, ky/S_0, 1/m
l	serration wavelength, m
l_y	spanwise turbulence lengthscale, $1.6V_c/\omega$, m
L	effective lift function, N/m
M	blade sectional flow Mach number
N_b	number of blades
N_r	number of rotors
n	mode number
OASPL	overall sound pressure level, dB (ref. 20 μPa)
R	rotor radius, m
r	span radial location, m
r_o	observer distance, m

RPM	revolution per minute
S_{pp}	acoustic PSD, Pa^2/Hz
SPL	sound pressure level, dB (ref. 20 μPa)
V	blade sectional freestream velocity, m/s
V_∞	rotor forward velocity, m/s
V_c	convection velocity, $0.7V$, m/s
V_{tip}	rotor tip speed, m/s
$\vec{x}$	observer position, m
X, Y, Z	coordinates in airfoil section frame, m
X_2, Y_2, Z_2	observer global coordinate, m
α	angle of attack, deg
α_{sh}	rotor shaft angle of attack, deg
μ	rotor advance ratio, $V_\infty \cos\alpha_{sh}/\Omega R$
Δr	blade section span, m
Ω	rotational speed, rad/s
ω	angular frequency, rad/s
Φ_{pp}	surface pressure spectrum, Pa^2/Hz
ϕ_o	observer elevation angle, deg
ψ_o	observer azimuth angle, deg
θ_o	observer angle to the trailing edge, deg

INTRODUCTION

Noise is a significant issue in rotorcraft applications (Ref. 1). For conventional helicopters, the noise levels are regulated (Ref. 2). In urban air mobility (UAM) aircraft, noise is a potential major barrier to market success, mainly due to public opposition (Ref. 3). UAM companies are committed to reducing their aircraft noise (Refs. 1, 4, 5). The main source of community noise from rotorcraft is aerodynamic noise from rotor blades, which is divided into tonal and broadband noise. Rotor tonal noise includes thickness noise, steady loading noise, high-speed impulsive noise (Ref. 6), and blade vortex interaction (BVI) noise (Refs. 7–10), and is crucial for both in-plane and out-of-plane observers. Rotor broadband noise, which includes blade-wake-interaction (BWI) noise (Refs. 11, 12) and airfoil-self noise (Ref. 13), is mainly pertinent for out-of-plane observers and falls within the human hearing's sensitive frequency range. During high-speed forward flight and hovering, where blade wake interactions are less pronounced, airfoil-self noise becomes the primary source of broadband noise (Ref. 14).

Rotorcraft noise reductions can be achieved by operation and design. During a rotorcraft operation, noise can be reduced by adjusting the flight path and vehicle attitude (Refs. 15–17), including increasing the flight altitude, avoiding populated areas, or decreasing the descending flight angle. On the other hand, noise reduction can be implemented during the rotorcraft design phase. The rotor tip speed and the number of blades can be varied to reduce tonal and broadband noise (Refs. 18–20). The tail rotor noise can be eliminated by the NOTAR-style tailboom system (Ref. 21). Swept and tapered blades at the rotor tip are widely adopted to reduce BVI noise (Refs. 22, 23). In addition, turbulent boundary layer trailing-edge broadband noise (Ref. 24) can be attenuated by turbulent hydrodynamic energy reduction or acoustic scattering modification. These modifications include active flow controls (Ref. 25), finlets (Ref. 26), porous material (Refs. 27, 28), and edge serrations (Refs. 29–31). Leading-edge serrations were also experimentally shown to reduce blade-vortex interaction noise (Ref. 32).

Among the aforementioned broadband noise reduction techniques, serrated blades are preferred on vertical flight rotors. The serrations are easy to manufacture, and the rotor performance remains unchanged after adding the serrated edges (Ref. 33). Regarding the mechanism of the noise reduction, on properly designed serrations, destructive interference can be achieved between the serration root and tip, and the acoustic energy is redistributed to the high cut-off modes (Ref. 29). Although serrations have been widely used on wind turbines to reduce trailing-edge noise (Ref. 34), the application of this idea to vertical flight rotors is still limited. The drone rotors with serrated trailing edges are experimentally shown to have noise reductions at high frequencies (Refs. 35,36). However, rapid design tools with proper analytical models to investigate the potential to reduce rotor broadband noise are still lacking. Therefore, the current study will focus on the analytical predictions of rotor broadband noise reduction with serrated trailing edges. The exact reason for noise reduction with serrated trailing edges is controversial. Experiments (Ref. 37) and high-fidelity numerical simulations (Ref. 38) were performed to show that the wall pressure spectrum can be significantly varied upstream a trailing edge with the serrations, which results in trailing-edge noise. It is possible that both source and scattering effects may play a role in noise reduction. However, the current research focuses on the acoustic scattering effect by serrations rather than the noise source effect, which has been more traditionally accepted.

The early work of Howe used the tailored Green's function to theoretically predict trailing-edge noise of the serrated blade (Ref. 39), but this method was shown to over-predict the noise reduction (Ref. 40). Using the Schwarzschild method (Ref. 41) and the Wiener-Hopf method (Ref. 42), Lyu et al. (Ref. 40) and Huang (Ref. 43) derived more recent serrated trailing-edge noise models, respectively. However, these two models cannot be solved exactly and require extensive computational time for the entire rotor blade. Using the Wiener-Hopf method, Ayton (Ref. 29) developed a new model that can be solved exactly with the infinite number of scattering modes, where any serrated shapes can be expressed in a 2-D function. To further reduce the computational cost, Lyu and Ayton (Ref. 44) simplified Ayton's model (Ref. 29) by implementing the finite number of cut-on and cut-off modes.

In this research, Lyu and Ayton's model (Ref. 44) will be modified to predict trailing-edge noise from the serrated rotor. This model requires the wall pressure fluctuations upstream of the trailing edge, which can be obtained from Lee's wall pressure spectrum model (Ref. 45). Lee's model is suitable for adverse pressure gradient flows. An underlying assumption in Lyu and Ayton's model is that the boundary layer formation upstream of a trailing edge is not affected by the appearance of the serration geometries. This was confirmed by Direct Numerical Simulation (DNS), showing that the wall pressure spectrum change upstream of a trailing edge is negligible with the addition of the serrations (Refs. 46, 47). The boundary layer parameters used to calculate the wall pressure spectrum are obtained from the software XFOIL using the panel method (Ref. 48), where the two-equation boundary layer formations are used to calculate a turbulent boundary layer flow around an airfoil surface. As for the rotor aerodynamics, the hovering flight is solved using the blade element momentum theory (BEMT), while the forward flight is solved by coupling the blade element theory (BET), Peters-He dynamic inflow model (Ref. 49), and the moment-balance trim solution (Ref. 50).

The current study will extend the capabilities of the rotorcraft broadband noise prediction tool, UCD-

QuietFly (Ref. 51), from a straight trailing edge to a serrated trailing edge. For the straight blade sections, Amiet's model (Refs. 52–54) is transformed into the rotor blade coordinates (Refs. 55, 56) to predict trailing-edge noise. Amiet's model uses the Schwarzschild method (Ref. 41) to solve an acoustic scattering by a trailing edge (Ref. 57). For the serrated sections, modified Lyu and Ayton's model is used. Note that a user-defined blade geometry accepts a blend of straight and serrated shapes on a rotor blade.

The current study will first validate this developed toolchain for serrated wing sections and serrated rotor blades against existing experimental data. Second, various parameters, including the serration number, shapes, and locations, will be compared for rotor broadband noise reduction capabilities. Finally, a quadrotor and a quiet helicopter design will be used to demonstrate the effectiveness of noise reduction with trailing-edge serrations in the context of UAM operations.

METHOD AND FORMULATION

The straight blade sections are calculated using Amiet's trailing-edge model (Ref. 52) improved by Roger and Moreau (Refs. 53, 54), which reads as

$$S_{pp}(\vec{x},\omega) = 4\left(\frac{kcZ}{8\pi S_0^2}\right)^2 2\Delta r|L|^2\Phi_{pp}(\omega)l_y(\omega,k_y) \tag{1}$$

where $S_0^2 = X^2 + \beta^2(Y^2 + Z^2)$, $\beta^2 = 1 - M^2$, k is the acoustic wavenumber, c is the chord length, Δr is the blade sectional span, L is the acoustic transfer function, l_y is the spanwise correction length, and Φ_{pp} is the wall pressure spectrum (Refs. 45, 58). The value of S_{pp} calculated in Eq. (1) is four times greater than that in the original Amiet model. This increase is due to the fact that scattering on one surface affects both surfaces of an airfoil section, effectively doubling the contribution to the scattered acoustic pressure (Ref. 53).

The spanwise correction length of the wall pressure spectrum is calculated using Corcos's model (Ref. 59) as

$$l_y(\omega,k_y) = \frac{\omega/(V_c b_c)}{k_y^2 + \omega^2/(V_c b_c)^2} \tag{2}$$

where the empirical constant b_c is a taken as 1.6, suggested in Ref. 60.

The acoustic transfer function L includes the contributions from the trailing-edge scattering L_1 and the leading-edge back-scattering L_2, such that $L = L_1 + L_2$. The current research added a correction term in L_1, which is the last term in Eq. (3) in order to ensure that a factor of 4 that was described earlier is only applied to the scattering part, but not to the incident part (Ref. 61).

$$L_1 = -\frac{e^{2iC}}{iC}\left\{(1+i)e^{-2iC}\sqrt{\frac{B}{B-C}}E^*[2(B-C)] - (1+i)E^*[2B] + 1 - e^{-2iC} + \frac{e^{-2iC}}{4}\right\} \tag{3}$$

$$B = \bar{K}_x + M\bar{\mu} + \bar{\kappa} \tag{4}$$

$$C = \bar{K}_x - \bar{\mu}(X/S_0 - M) \tag{5}$$

For straight blades, Roger and Moreau's leading-edge back-scattering correction (Ref. 53) is given in Eq. (6). This term is important for small chord lengths and low frequencies, where the Helmholtz number based on the chord length, kc, is small.

$$\frac{1}{H}L_2 = \left\{e^{4i\bar{\kappa}}[1-(1+i)E^*(4\bar{\kappa})]\right\}^c - e^{2iD} + i[D + k_x^* + M\bar{\mu} - \bar{\kappa}]G \tag{6}$$

where

$$H = \frac{(1+i)e^{-4i\bar{\kappa}}(i-\Theta^2)}{2\sqrt{\pi}(\alpha-1)k_x^*\sqrt{B}} \tag{7}$$

$$D = \bar{\kappa} - \bar{\mu}X/S_0; \quad \alpha = V/V_c \tag{8}$$

$$\Theta = \sqrt{\frac{\bar{K}_x + \bar{\mu}M + \bar{\kappa}}{k_x^* + \bar{\mu}M + \bar{\kappa}}} \tag{9}$$

$$
\begin{aligned}
G = & (1+\epsilon)e^{i(2\bar{\kappa}+D)}\frac{\sin D - 2\bar{\kappa}}{D-2\bar{\kappa}} + (1-\epsilon)e^{i(-2\bar{\kappa}+D)}\frac{\sin D + 2\bar{\kappa}}{D+2\bar{\kappa}} \\
& + \frac{(1+\epsilon)(1-i)}{2(D-2\bar{\kappa})}e^{4i\bar{\kappa}}E^{*}(4\bar{\kappa}) - \frac{(1-\epsilon)(1+i)}{2(D+2\bar{\kappa})}e^{-4i\bar{\kappa}}E^{*}(4\bar{\kappa}) \\
& + \frac{e^{2iD}}{2}\sqrt{\frac{2\bar{\kappa}}{D}}E^{*}(2D)\big[\frac{(1+i)(1-\epsilon)}{D+2\bar{\kappa}} - \frac{(1-i)(1+\epsilon)}{D-2\bar{\kappa}}\big]
\end{aligned}
\tag{10}
$$

and the imaginary part of $\{\}^c$ in Eq. (6) is multiplied by $\epsilon = (\sqrt{1+1/(4\bar{\mu})})^{-1}$.

For the serrated blade sections, the original Lyu and Ayton model (Ref. 44) reads

$$
S_{pp} \approx \frac{\bar{k}}{2\pi r_o}\sin^2\frac{\theta_o}{2}\frac{\chi+\bar{k}}{2\left(\chi-\bar{k}\cos\theta_o\right)^2}\sum_{n=-\infty}^{+\infty}\Pi(\omega,k_y)|E_n(\lambda)|^2 \tag{11}
$$

where the observer location, in terms of r_o and θ_o are shown in Fig. 1. The observer angle, θ_o, is defined in the $X-Z$ plane, and the spanwise location is not considered in the original model.

The current study proposes corrections to this equation to implement Lyu and Ayton's model into rotor cases. First, to eliminate the limitation of the unit span length assumption, the blade section span length, Δr, is multiplied in Eq. (11) in order to account for the blade sectional length. Second, to match the attenuation rate of the spherical acoustic propagation, Eq. (11) is divided by the observer distance, r_o. Third, the effect of the spanwise observer location is included in $r_o^2 = (x/\beta)^2 + y^2 + z^2$ as well as in the spanwise wavenumber, such that $k_y = 2\pi n/l + ky/S_0$. In the original model, r_o^2 and k_y were defined as $(x/\beta)^2 + z^2$ and $2\pi n/l$, respectively (Ref. 44). Fourth, a factor of four is added to correct the scattering effect on the upper and lower surfaces, which is similar to Eq. (1). Note that these modifications are physics-based corrections instead of thorough analytical derivations. Thus, the accuracy of these modifications will be validated later. The final new equation used is given as

$$
S_{pp} \approx \frac{4\Delta r\bar{k}}{2\pi r_o^2}\sin^2\frac{\theta_o}{2}\frac{\chi+\bar{k}}{2\left(\chi-\bar{k}\cos\theta_o\right)^2}\sum_{n=-\infty}^{+\infty}\Pi(\omega,k_y)|E_n(\lambda)|^2 \tag{12}
$$

where the wavenumber-frequency wall pressure spectrum is

$$
\Pi(\omega,k_y) = \frac{1}{\pi}\Phi_{pp}(\omega)l_y(\omega,k_y) \tag{13}
$$

$\bar{k} = k\beta$ is the the mean-flow-corrected acoustic wavenumber, θ_o the observer angle, $\chi = \bar{k}_x\beta$ the corrected convective wavenumber, $\bar{k}_x = k_x + kM/\beta^2$, $\lambda = (\bar{k}_x - \bar{k}\cos\theta)\bar{c}/4$, which is an input to the radiation function $E_n(\lambda)$ (Ref. 62), and $\bar{c} = 2h/\beta$ the corrected serration amplitude. Note that the fundamental mode of $n = 0$ is the most important modal term, and the effects of the higher modes appear when $k/\beta > 2n\pi$. The radiation function of the serrated geometry is given in Eq. (14).

$$E_n(\lambda) = \int_0^1 e^{i\bar{c}F(\eta)(\bar{k}_x+\lambda)} e^{-i2\pi n\eta} d\eta \tag{14}$$

where $F(\eta)$ is the non-dimensional height of the serrations, and η is zero at the root and one at the tip of a blade serration. $2h$ and l are used to denote the dimensional peak-to-peak amplitude of the serration and the serration wavelength, respectively, for future usages in the current study, as shown in Fig. 2. This function provides the flexibility to describe arbitrary serration geometries, including a blend of straight and serrated trailing edges. The selected trailing-edge serrated geometries are plotted in Fig. 3, where their corresponding equations are given in Eq. (16). The geometry equations describe the serration height $F(\eta)$ as a function of the η coordinate within a wavelength of l, where the origin of the $F - \eta$ coordinate is located at the lower-left corner.

The sound pressure level (SPL) is calculated from the power spectrum density S_{pp} as

$$\text{SPL} = 10\log_{10}\left(\frac{2\pi S_{pp}}{(2\times 10^{-5})^2}\right) \tag{15}$$

The starting blade radial location and shape of the serration can be customized, as shown in Fig. 2. Although a straight blade can be calculated in the modified Lyu and Ayton's model, Amiet's trailing-edge noise model is much faster when used on straight sections. In the current study, a rotor blade is segmented into 40 sections of equal length. The rotor design and operational parameters, such as the collective and cyclic pitches, blade twist, forward speed, and multi-rotor hub locations, are included in the blade section coordinate transformations (Ref. 55). It is assumed that the serration does not affect the blade chord length in aerodynamic simulations.

$$F_{Saw-tooth} = \begin{cases} 2\eta - 0.5, & 0 < \eta < 0.5 \\ 1.5 - 2\eta, & 0.5 < \eta < 1 \end{cases} \tag{16a}$$

$$F_{Square} = \begin{cases} 0.5, & 0 < \eta < 0.25 \\ -0.5, & 0.25 < \eta < 0.75 \\ 0.5, & 0.75 < \eta < 1 \end{cases} \tag{16b}$$

$$F_{Sine} = 0.5 \sin 2\pi\eta, \quad 0 < \eta < 1 \tag{16c}$$

$$F_{Half-sine} = 0.5 \sin \pi\eta, \quad 0 < \eta < 1 \tag{16d}$$

$$F_{Ogee} = \begin{cases} 4\eta - 0.5 - \sin \pi\eta, & 0 < \eta < 0.5 \\ 3.5 - 4\eta) - \sin \pi\eta, & 0.5 < \eta < 1 \end{cases} \tag{16e}$$

$$F_{Chopped\, peak} = \begin{cases} 10/3\eta, & 0 < \eta < 0.15 \\ 0.5, & 0.15 < \eta < 0.35 \\ 11/8 - 5/2\eta, & 0.35 < \eta < 0.75 \\ 2\eta - 2, & 0.75 < \eta < 1 \end{cases} \tag{16f}$$

$$F_{Slitted\, U-root} = \begin{cases} 2\eta, & 0 < \eta < 0.25 \\ 0.94 - 1.78\eta, & 0.25 < \eta < 0.7 \\ 2.5 - 4\eta, & 0.7 < \eta < 0.75 \\ -3.5 + 4\eta, & 0.75 < \eta < 0.8 \\ -1.5 + 1.5\eta, & 0.8 < \eta < 1 \end{cases} \tag{16g}$$

$$F_{Slitted\, U-root} = \begin{cases} 2\eta, & 0 < \eta < 0.25 \\ 0.94 - 1.78\eta, & 0.25 < \eta < 0.7 \\ -0.5, & 0.7 < \eta < 0.8 \\ -1.5 + 1.5\eta, & 0.8 < \eta < 1 \end{cases} \tag{16h}$$

In the current study, the boundary layer parameters are calculated using the XFOIL panel method code (Ref. 48), the wall pressure spectrum near the blade trailing edge using Lee's model (Ref. 45), the hovering flights using blade element momentum theory (BEMT), the forward flights using an in-house low-fidelity rotor comprehensive code (Ref. 63), and trailing-edge noise using UCD-QuietFly (Refs. 19, 51, 55, 64). Note that the boundary layer parameters can be alternatively found using Reynolds-Averaged Navier-Stokes (RANS) (Refs. 65–67). A flow chart of this method of serrated rotor aerodynamics and broadband noise predictions is shown in Fig. 4.

Validations

First, Amiet's model (Ref. 52) is compared with the modified Lyu and Ayton's model (Ref. 44) for the calculations of trailing-edge noise on the straight wing section. Second, the broadband noise of two serrated-blade rotors, one in hovering flight and the other in forward flight, is calculated in UCD-QuietFly and validated against the experiments.

Aerodynamic tools used in the current study, involving the blade element momentum theory (BEMT) and the blade element theory (BET), were validated in previous publications (Ref. 19, 68). Additionally, the validations of the wall pressure spectrum model were given in Ref. 45.

Serrated Wing Section

Verifications and validations of the broadband noise predictions for straight and serrated wing sections and straight and serrated rotors are presented. Table 1 shows two verification cases and one validation case. The first verification case result is shown in Fig. 5(a), where the modified Lyu and Ayton's model is used to predict trailing-edge noise of a straight wing section, which is compared to the results of Amiet's model. The overlapping of these two models demonstrates the correctness of our improvements shown in Eq. (12). The comparisons validate the effectiveness of changing observer distance by adding an attenuation rate of $1/r_o$ to the original Lyu and Ayton's model. The modifications of the spanwise wavenumber and the finite span in the current study demonstrate that the serrated trailing-edge noise model reduces to Amiet's trailing-edge noise model when used on a straight airfoil section.

Figure 6 shows the effect of the spanwise wavenumber k_y on a straight wing, where the original Lyu and Ayton's model used $k_y = 2n\pi/l$ that did not account for the change of observer locations in the spanwise direction. The modified spanwise wavenumber of $k_y = ky/S_0 + 2\pi n/l$ is shown to give better agreements with the Amiet model on a straight trailing edge for observers at non-zero spanwise locations. This modification is important in rotorcraft applications since the observers of interest can be located in the in-plane directions.

The predictions of trailing-edge noise of a serrated wing and a straight wing are provided in Fig. 7, where the experiment data is given (Ref. 69). The noise reduction, ΔSPL (sound pressure level), is the decibel difference between a straight blade and a serrated blade in the same condition. The positive ΔSPL indicates the noise reduction. Amiet's model was used on the straight blade, while the modified Lyu and Ayton's model was used on the serrated blade in this validation study. It is seen that noise reduction is predicted well at mid-frequencies. The over-predictions of the noise reduction are observed in the high-frequency range, which is likely due to other noise sources in the experiment that are not included in the current acoustic model, such as misaligned small vortical flows at the serration root sections (Ref. 70). The existence of these additional sources is case-dependent. The over-prediction of the noise reduction was also present in the original Ayton's paper (Ref. 29).

Serrated Rotor

A hovering rotor validation case is provided in Table 2, where an APC drone rotor is serrated from the mid-span to the tip. The experiment of a hovering rotor was conducted in the University of Bristol's anechoic chamber; the saw-tooth trailing edge was cut on the APC 11x4.7 Slow Flyer rotor, and a microphone array was installed to collect the acoustics data (Ref. 35). The microphone is 1.65 m directly above the rotor hub. The predictions of the rotor noise with straight and serrated trailing edges are given in Fig. 8. The predictions of the straight-blade rotor noise match the experiment very well. At the mid to high frequencies, the predictions of the serrated rotor noise give reasonable noise reductions compared to the experiment, while some under-predictions appear. In the low-frequency range, both the straight rotor and serrated rotor noise levels are over-predicted when using Lyu and Ayton's model. It is found that blades with chord lengths larger than 0.1 m do not have this over-prediction issue at low frequencies. Overall, although the serrated trailing-edge noise predictions have discrepancies compared to the experiment, they give reasonable predictions for noise reduction. Discrepancies are also observed on the straight blade at the high-frequency range between the Amiet model and the modified model, which is not consistent with the trend found on an airfoil section by Santamaria et al. (Ref. 31). This inconsistency is likely due to the effects of low observer angles on the twisted rotor blade, which deserves future investigations.

In addition to the broadband noise validation of a hovering rotor, broadband noise is predicted on a forward-flight eHANG rotor with serrated trailing edges. The eHANG drone rotor parameters are provided in Table. 2, where the acoustic measurements were taken in an anechoic wind tunnel (Ref. 36). The microphone is in the forward direction of the rotor, with an elevation angle of -56.31°, azimuthal angle of 180°, and a distance of 1.49 m. The tested rotor has saw-tooth serrations with a height-to-wavelength ratio, $2h/l$, of 0.5. The noise reduction between a serrated-blade rotor and a straight-blade rotor is predicted in Fig. 9 and compared against the experimental data. It is seen that the prediction has good agreement with the measurements, especially above 5 kHz, where apparent noise reductions are present.

Results

First, the serration effects on rotor broadband noise are assessed by varying the trailing-edge serration parameters: the number of serrations, serrations' starting radial location, serration geometry, and serration height. Next, the trailing-edge serrations are applied to two NASA UAM eVTOL vehicles: quadrotor and quiet helicopter. Quadrotor noise is compared between the straight blade and serrated blade with varying tip speeds and blade numbers. The hemisphere directivity is compared with the two designs. A quiet helicopter in forward flight is studied for serrated blades and straight blades.

Effects of Serration Parameters

The baseline rotor case is an APC Slow Flyer drone rotor with serrated trailing edges, where the parameters are given in Table. 2. For each parameter studied, other parameters are kept as the baseline values. In this parameter study, the straight-blade rotor noise prediction is used as a reference, which is calculated using the modified Lyu and Ayton's model from the corresponding serration region outboard and using Amiet's model inboard. The purpose of this practice is to reduce computational time using the faster Amiet's model for the inboard straight sections, which are less important acoustically. The noise difference between the straight-blade rotor and serrated-blade rotor (ΔOASPL) is calculated. Note that the current research uses the modified Lyu and Ayton's model even for the straight blade at the outboard sections where the serrations would be located so that the noise comparison between the straight blade and the serrated blade is fair. The frequency range of summation for OASPL (overall sound pressure level) is 0.1-13 kHz.

The effect of varying the number of serrations is shown in Fig. 10, where the rotor trailing edges have saw-tooth serrations from its 50 % radial position to the tip. As the number of serrations increases, the serration wavelength is shortened, which can also be seen as the effect of changing the serration wavelength. The frequency spectrum of SPL in Fig. 10(a) shows that noise reductions occur in the mid- to high-frequency range (above 2.5 kHz), while a slight noise increase is seen in the low frequencies. Increasing the number of serrations (or reducing the serration wavelength) reduces the noise level. With more serrations or the shorter wavelength, the destructive interference on the rotor blade is increased since the modal coefficient in Eq. (14) gets more oscillations with more serrations on the blade span. However, as more serration shapes are added, the effectiveness of noise reduction is reduced. This observation is consistent with the experimental measurements taken on serrated airfoil sections (Ref. 71). Therefore, considering the manufacturing and structural challenges, 22 serrations ($2h/l$=2) are desirable among the tested cases, although more serrations slightly improve the noise reduction.

Figure 11 shows the effect of changing the starting radial position of the serrations, where the inboard of the starting position has straight edges, as shown in Fig. 2. For example, serration root r/R of 90% means that the serration starts at the 90% span and ends at the tip. The frequency spectrum indicates that the noise levels at the mid and high frequencies (above 2 kHz) are reduced with increasing the span portion of the serrated blade, while the low-frequency range has a slight noise increase. This low-frequency noise increase might result from the model difference when blending Amiet's model and Lyu and Ayton's model on the same blade, as some discrepancies between the two models were present at low frequencies in Fig. 8. The benefit of using Amiet's model for the straight portion of a blade is the reduction of the computational time. The trend of the noise reduction shows that the noise level of the serrated rotor keeps decreasing as the starting position of the serrations moves to the root, but the tip serrations are more effective in reducing noise since the higher flow speeds at the tip sections give the higher noise levels. The most outboard 10% sections provide a noise reduction of 1.56 dB, and the 70-90% and the 50-70% sections each provide noise reductions of approximately 2 dB. However, the 30-50% sections give a noise reduction of less than 1 dB, and the inboard 30% sections have minimal noise reduction benefits. Thus, it is suggested that using trailing-edge serrations starting from 50% r/R is preferred considering noise benefit and manufacturing difficulty.

Figure 12 demonstrates the effect of increasing the serration height on broadband noise. The APC Slow Flyer rotor has a chord length of approximately 28 mm at 75% r/R, so attaching a too-large serration height is unrealistic. Since the serrations are attached to the blade trailing edges, this approach results in increasing the blade chord length. The impacts of varying the chord length on the boundary layer flows are neglected in this study. It is observed that increasing the serration height has noticeable benefits of noise reduction, but this benefit is reduced at the larger serration heights. As the serration height increases, the incline angle between the serration and the blade span also increases to create stronger destructive interference between the serration tip and root regions. Note that the results depend on the ϕ_{pp} and l_y obtained from the clean airfoil. The trend of changing the height to wavelength ratio $2h/l$ in Fig. 12 is the same as in Fig. 10; the higher $2h/l$ increases the noise reduction at a decreasing rate. This result is consistent with the simulations on serrated airfoil sections by Kholodov and Moreau (Ref. 62). In addition, more acoustic energy is redistributed to the higher-frequency cut-off modes (imaginary part of E_n) since the shape coefficient in Eq. 14 is a function of $k\bar{c} = 2kh/\beta$, which is proportional to the serration height.

The different serration shapes shown in Fig. 3 and Eq. (16) are used on the rotor to study their noise reduction capabilities. Figure 13 shows that the sine-wave shape gives the largest noise reduction, and the chopped peak and the saw-tooth shapes give similarly excellent noise reductions. On serrated airfoil sections, Kholodov and Moreau also found the optimal shapes to be close to the saw-tooth (Ref. 62). The square and the half-sine shapes give the least noise reductions of approximately 3 dB. In Figs. 13(a) and 13(b), where the saw-tooth shape gives an increasing noise reduction as the frequency increases, but the square shape provides an up-and-down noise reduction behavior as a function of frequency. Note that the saw-tooth shape in Fig. 13(a) appears to have more noise reduction than the sine shape, specifically above 4 kHz. This trend is not reflected in the ΔOASPL plot since the noise levels above 4 kHz for the saw-tooth and sine shapes are very small compared to the low-frequency noise. The variations in noise reduction for different geometries are reflected in the modal coefficients in Eq. (16), which describe the far-field destructive interference between the tip and the root. In the case of serrated wing sections, this interference manifests as oscillations in the frequency domain noise level. However, for rotors with serrated blades, this oscillatory effect is less pronounced due to the presence of multiple sections and blade rotation.

Noise Reduction on an eVTOL Quadrotor

The UAM quadrotor conceptual designs by NASA (Ref. 72) shown in Fig. 14 are studied for their noise reduction potentials using trailing-edge serrations. The vehicle is operated in hovering condition, and the observer is 492 ft (150 m) directly below the quadrotor center. The detailed parameters of the vehicle can be found in Table. 2. In this study, the blade trailing edges of the quadrotor are serrated from mid-span to the tip with the saw-tooth geometry, where serration height is $2h$ = 0.0702 m and serration wavelength is l=0.0351 m so that $2h/l$ becomes 2. In the computer program UCD-QuietFly, the serration shape function in Eq. 16 is discretized into 100 spanwise points per serration. The converged solution was found by summing the mode number, n in Eq. 12, from -10 to 10. For the straight-blade quadrotors, Amiet's model is used on the entire blade span. For reference, the blade chord length at 75% span is approximately 0.17 m. For this chord length, It was found that Amiet's model and the modified Lyu and Ayton's model provide almost the same results on the straight blade as demonstrated in Fig. 5(a). Thus, the current study has selected Amiet's model for its fast calculation. Three designs, with different tip speeds (700, 550, and 375 ft/s) and numbers of blades (3 and 7), are studied in Fig. 15. The selection of the tip speed and blade number is the same as a quadrotor acoustic study by Kottapalli and Silva (Ref. 73). The community background noise measured in a neighborhood in Sunnyvale, California (Ref. 74) is added to the figure as a reference.

The noise spectrum shows that the noise reductions appear in the entire frequency range. ΔOASPL shows that the trailing-edge serrations have more noise reductions on the higher-tip-speed and fewer-blade designs. Trailing-edge serrations are effective in reducing noise in the mid-frequency range (1-5 kHz), which is masked by the community background noise. Although the high-frequency noise with serrations is not entirely masked by the background noise, the noise level, even in the loudest condition, is lower than 40 dB, which will help have the UAM aircraft much more favorably received by the public. In summary, using trailing-edge serrations as a noise reduction technique, multi-rotor eVTOL aircraft have the potential to reduce broadband noise by more than 9 dB, as shown in Fig. 15(b), which is significant considering the unmasked eVTOL noise in the urban environment (Ref. 51).

The hemispheric broadband noise directivities of the UAM eVTOL quadrotor are shown in Fig. 16, including the straight-blade quadrotor, the serrated-blade quadrotor, and the noise reduction. The vehicle parameters were given in Table 2, and the radius of the observer hemisphere is 150 m. The quadrotor selected for this directivity study has three blades and a tip speed of 700 ft/s. The blue dot in Fig. 16 represents the vehicle position. The straight-blade quadrotor noise is calculated using Amiet's model. It is seen that both the straight-blade and the serrated-blade quadrotors have dipole directivity, where the highest noise level is found directly below the quadrotor. The noise reduction is observed for almost all observer locations on the hemisphere, except for the very small elevation angles (in-plane) due to the model difference at low frequencies. This directivity pattern on serrated-blade rotorcraft is consistent with the directivity on a serrated airfoil section, where noise reductions are observed for all observer angles (Refs. 29, 75).

Noise Reduction of a Quiet Helicopter in Cruise

The NASA single-rotor quiet helicopter in forward flight shown in Fig. 17 is analyzed for its broadband noise reduction using serrated trailing edges. This quiet helicopter (Ref. 18) design has a muffled propulsion system and a NOTAR-style tailboom to eliminate high-frequency tail rotor noise. The quiet helicopter parameters are given in Table 2, where the design of 700 ft/s tip speed is studied. The detailed aerodynamic predictions for the quiet helicopter and parameter input can be found in Ref. 19. In the UCD-QuietFly simulation, the number of discrete points per serration is 150, and the modes are summed from -5 to 5. For simple geometries, such as saw-tooth, it is found that these selections of discretization and modes are sufficient to get converged solutions.

The broadband noise hemisphere directivities of the quiet helicopter are given in Fig. 18, where $-X_2$ is the forward direction. It is seen that due to the forward tilting angle, the hemisphere directivities are tilted in the forward direction. Both the straight rotor and the serrated rotor have the dipole directivity. Figure 18(c) shows that the highest noise reduction occurs in the forward direction (-45° elevation angle), although the downward direction also shows a significant noise reduction by 10 dB.

Conclusions

The current study presented a state-of-the-art approach to predict broadband noise generated from rotors with serrated trailing edges. The original Lyu and Ayton's serrated airfoil section model, based on the Wiener-Hopf solution, was extended to include the finite span, far-field noise attenuation, modified scattering coefficient, and spanwise observer distance. These extensions were verified with Amiet's model and validated for serrated trailing-edge noise of a wing section, a hovering rotor, and a forward rotor. The effects of serration parameters on rotor broadband noise were studied. The broadband noise directivities of a serrated-blade quadrotor and quiet helicopter were investigated. The potential noise reduction using serrated trailing edges on the UAM eVTOL vehicles was analyzed. For the specific cases considered in the present study, important findings are summarized as follows:

- The serration height to wavelength ratio of 2 is a desirable selection to reduce rotor broadband noise since further increasing the ratio only has slight noise reduction benefits. The optimal radial range for installing trailing-edge serrations on a rotor blade is from 50% to the blade tip. While the addition of spanwise serrations enhances noise reduction, incorporating serrations on less than the inner 50% of the rotor blade results in only marginal noise reduction. The sine-wave, chopped peak, and saw-tooth serration shapes provide the largest noise reductions, and the square shape provides the least noise reduction among the studied shapes.

- On an eVTOL quadrotor, more than 9 dB noise reduction was found with serrated trailing edges. Higher noise reductions were observed on the serrated quadrotors with higher tip speeds and fewer blades. The serrated-blade UAM eVTOL quadrotor had the dipole broadband noise directivity, and noise reductions were observed at all observer angles with a primary noise reduction toward the downward direction.

- For a single-rotor NASA's quiet helicopter in forward flight, approximately 10 dB noise reduction was observed in the downward direction, and the maximum noise reduction occurred in the forward direction.

Although this research is focused on analytic and low-fidelity predictions of serrated trailing-edge noise, the results provide insights into important serration parameters in the context of rotor broadband noise and demonstrate the significant potential to reduce UAM aircraft noise. It is suggested in the future study that the serration parameters or geometries are optimized to maximize the noise reduction and the predictions are further validated against experimental data or high-fidelity computational fluid dynamics (CFD) predictions. It is also recommended that future research investigates the serrated trailing-edge noise model for small chord lengths and low frequencies, aiming to improve the current model's underestimations attributed to simplified assumptions used in the theoretical model such as frozen gust. Finally, the analytic model is found to only consider the destructive interferences, and it did not account for the acoustic source change due to the add-on serrations. This assumption and limitation can be revisited with more fundamental aeroacoustic research development.

References

[1]Holden, J., and Goel, N., "Fast-Forwarding to a Future of On-Demand Urban Air Transportation," *Uber Elevate White Paper*, 2016.

[2]Federal Aviation Administration, "Stage 3 Helicopter Noise Certification Standards - 14 CFR Part 36," 2012.

[3]Hasan, S., "Urban Air Mobility (UAM) Market Study," NASA RP HQ-E-DAA-TN63497s, 2018.

[4]Bain, J., Mikic, G., and Stoll, A., "Aerodynamic And Acoustic Design Of The Joby Aviation eVTOL Propeller," Proceedings of the Vertical Flight Society 77th Annual Forum, Virtual Event, May 11-13, 2021.

[5]Huff, D. L., Henderson, B. S., Cluts, J. D., Boyle, D. K., Bennett, J., and Janzen, J., "Noise Measurements from Ground Tests of the Moog SureFly Vehicle," AIAA 2021-2209, Proceedings of the 2021 AIAA Aviation Forum, Virtual Event, August 2-6, 2021.

[6]Lee, S., Brentner, K., and Morris, P., "Long-Range and Nonlinear Propagation of Helicopter High-Speed Impulsive Noise," *Journal of the American Helicopter Society*, **62**, 022007(2017), DOI: 10.4050/JAHS.62.022007.

[7]Jia, Z., Lee, S., Sharma, K., and Brentner, K., "Aeroacoustic Analysis of a Lift-Offset Coaxial Rotor Using High-Fidelity CFD/CSD Loose Coupling Simulation," *Journal of the American Helicopter Society*, **65**, 012011(2020), DOI: 10.4050/JAHS.65.012011.

[8]Jia, Z., and Lee, S., "High-Fidelity Computational Analysis on the Noise of a Side-by-Side Hybrid VTOL Aircraft," *Journal of The American Helicopter Society*, **67**, 022005(2022), DOI: 10.4050/JAHS.67.022005.

[9]Jia, Z., and Lee, S., "Computational Study on Noise of Urban Air Mobility Quadrotor Aircraft," *Journal of The American Helicopter Society*, **67**, 012009(2022), DOI: 10.4050/JAHS.67.012009.

[10]Sagaga, J., and Lee, S., "Acoustic Predictions for the Side-by-Side Air Taxi Rotor in Hover," Proceedings of the Vertical Flight Society 77th Annual Forum, Virtual Event, May 11-13, 2021.

[11]Brooks, T., and Burley, C., "Blade Wake Interaction Noise for a Main Rotor," *Journal of the American Helicopter Society*, Vol. 49 (1), 2004, pp. 11–27, DOI: 10.4050/JAHS.49.11.

[12]Li, S., "An Analytic Method to Predict Rotor BladeWake Interaction Noise," Proceedings of the Vertical Flight Society 79th Annual Forum, West Palm Beach, FL, May 16-18, 2023.

[13]Brooks, T., Pope, D., and Marcolini, M., "Airfoil Self-noise and Prediction," , 1989. NASA RP 1218.

[14]Brooks, T., Marcolini, M., and Pope, D., "Main Rotor Broadband Noise Study in the DNW," *Journal of the American Helicopter Society*, Vol. 34 (2), 1989, pp. 3–12, DOI: 10.4050/JAHS.34.2.3.

[15]Page, J., "In Situ Development and Application of Fly Neighborly Noise Abatement Procedures for Helicopters," Proceedings of the Vertical Flight Society 75th Annual Forum, Philadelphia, Pennsylvania, May 13–16, 2019.

[16]Greenwood, E., "Dynamic Replanning of Low Noise Rotorcraft Operations," Proceedings of the Vertical Flight Society 75th Annual Forum, Philadelphia, Pennsylvania, May 13–16, 2019.

[17]Krishnamurthy, S., Aumann, A. R., and Rizzi, S. A., "A Synthesis Plugin for Auralization of Rotor Self Noise," AIAA 2021-2211, Proceedings of the 2021 AIAA Aviation Forum, Virtual Event, August 2-6, 2021.

[18]Johnson, W., "A Quiet Helicopter for Air Taxi Operations," Proceedings of the 2020 VFS Aeromechanics for Advanced Vertical Flight Technical Meeting, San Jose, CA, January 21-23, 2020.

[19]Li, S., and Lee, S., "Acoustic Analysis and Sound Quality Assessment of a Quiet Helicopter for Air Taxi Operations," **67**, 032001(2022), DOI: 10.4050/JAHS.67.032001.

[20]Silva, C., and Johnson, W., "Practical Conceptual Design of Quieter Urban VTOL Aircraft," Proceedings of the Vertical Flight Society 77th Annual Forum & Technology Display, Virtual Event, May 10-14, 2021.

[21]Currier, J. M., Hardesty, M., and O'Connell, J. M., "NOTAR system - A quiet character," Proceedings of the AHS International Specialists' Meeting on Rotorcraft Basic Research, Philadelphia, PA, October 1991.

[22]Yu, Y., "Rotor Blade-Vortex Interaction Noise," *Progress in Aerospace Sciences*, Vol. 36, 2000, pp. 97–115.

[23]JanakiRam, R., Sim, B., Kitaplioglu, C., and Straub, F., "Blade-Vortex Interaction Noise Characteristics of a Full-Scale Active Flap Rotor," Proceedings of the American Helicopter Society 65th Annual Forum, Grapevine, Texas, May 27-29, 2009.

[24]Lee, S., Ayton, L., Bertagnolio, F., Moreau, S., Chong, T. P., and Joseph, P., "Turbulent boundary layer trailing-edge noise: Theory, computation, experiment, and application," *Progress in Aerospace Sciences*, Vol. 126, 2021, p. 100737.

[25]Szoke, M., and Azarpeyvand, M., "Active Flow Control Methods for the Reduction of Trailing Edge Noise," AIAA 2017-3004, Proceedings of the 23rd AIAA/CEAS Aeroacoustics Conference, Denver, Colorado, June 5-9, 2017.

[26]Shi, Y., and Lee, S., "Numerical Study of 3-D Finlets Using RANS CFD for Trailing Edge Noise Reduction," *International Journal of Aeroacoustics*, Vol. 19 (1-2), 2020, pp. 95–118.

[27]Ali, S. A. S., Szoke, M., Azarpeyvand, M., and da Silva, C. R. I., "Turbulent Flow Interaction with

Porous Surfaces," AIAA 2018-2801, Proceedings of the 2018 AIAA/CEAS Aeroacoustics Conference, Atlanta, Georgia, June 25-29, 2018.

[28]Moreau, S., Dignou, B., Jaiswal, P., Yakhina, G. R., Pasco, Y., Sanjose, M., Alstrom, B., and Atalla, N., "Trailing-Edge Noise of a Flat Plate with Several Liner-Type Porous Appendices," AIAA 2018-3119, Proceedings of the 2018 AIAA/CEAS Aeroacoustics Conference, Atlanta, Georgia, June 25-29, 2018.

[29]Ayton, L. J., "Analytic Solution for Aerodynamic Noise Generated by Plates with Spanwise-Varying Trailing Edges," *Journal of Fluid Mechanics*, Vol. 849, 2018, p. 448–466.

[30]Li, S., and Lee, S., "Extensions and Applications of Lyu and Ayton's Serrated Trailing-Edge Noise Model to Rotorcraft," AIAA 2022-2916, Proceedings of the 28th AIAA/CEAS Aeroacoustics Conference, Southampton, UK, June 14-17, 2022.

[31]Santamaria, J., Sanjose, M., and Moreau, S., "Fast Broadband Noise Prediction of Serrated UAV Rotors in Hover," AIAA 2023-0618, Proceedings of the 2023 AIAA SciTech Forum, National Harbor, MD, January 23-27, 2023.

[32]Feinerman, J., Koushik, S., and Schmitz, F., "Effect of Leading-Edge Serrations on Helicopter Blade–Vortex Interaction Noise," *Journal of The American Helicopter Society*, **62**, 032001(2017), DOI: 10.4050/JAHS.62.032001.

[33]Ning, Z., Wlezien, R. W., and Hu, H., "An Experimental Study on Small UAV Propellers with Serrated Trailing Edges," AIAA 2017-3813, Proceedings of the 2017 AIAA Aviation Forum, Denver, Colorado, 5-9 June, 2017.

[34]Oerlemans, S., Fisher, M., Maeder, T., and Kögler, K., "Reduction of Wind Turbine Noise Using Optimized Airfoils and Trailing-Edge Serrations," *AIAA Journal*, Vol. 47 (6), 2009, pp. 1470–1481.

[35]Cambray, A., Pang, E., Rezgui, D., Azarpeyvand, M., and Ali, S. A. S., "Investigation Towards a Better Understanding of Noise Generation from UAV Propellers," AIAA 2018-3450, Proceedings of the 2018 AIAA Aviation Forum, Atlanta, Georgia, June 25-29, 2018.

[36]Yang, Y., Wang, Y., Liu, Y., Hu, H., and Li, Z., "Noise Reduction and Aerodynamics of Isolated Multi-Copter Rotors with Serrated Trailing Edges During Forward Flight," *Journal of Sound and Vibration*, Vol. 489, 2020, p. 115688.

[37]Letica, S., and Alexander, W. N., "Understanding the Impact of a Serrated Trailing Edge on the Unsteady Hydrodynamic Field," *Journal of Aerospace Engineering*, Vol. 34 (4), 2021, p. 04021045.

[38]Gelot, M. B., and Kim, J. W., "Broadband Noise Prediction for Aerofoils with a Serrated Trailing Edge Based on Amiet's theory," *Journal of Sound and Vibration*, Vol. 512, 2021, p. 116352.

[39]Howe, M., "Noise Produced by a Sawtooth Trailing Edge," *The Journal of the Acoustical Society of America*, Vol. 90 (1), 1991, pp. 482–487.

[40]Lyu, B., Azarpeyvand, M., and Sinayoko, S., "Prediction of Noise from Serrated Trailing Edges," *Journal of Fluid Mechanics*, Vol. 793, 2016, p. 556–588.

[41]Landahl, M., *Unsteady Transonic Flows*, Pergamon Press, 1961.

[42]Noble, B., *Methods Based on the Wiener–Hopf Technique for the Solution of Partial Differential Equations*, Pergamon Press, 1958.

[43]Huang, X., "Theoretical Model of Acoustic Scattering from a Flat Plate with Serrations," *Journal of Fluid Mechanics*, Vol. 819, 2017, p. 228–257.

[44]Lyu, B., and Ayton, L. J., "Rapid Noise Prediction Models for Serrated Leading and Trailing Edges," *Journal of Sound and Vibration*, Vol. 469, 2020, p. 115136.

[45]Lee, S., "Empirical Wall-Pressure Spectral Modeling for Zero and Adverse Pressure Gradient Flows," *AIAA Journal*, Vol. 56 (5), 2018, pp. 1818–1829.

[46]Jones, L. E., and Sandberg, R. D., "Acoustic and Hydrodynamic Analysis of the Flow Around an Aerofoil with Trailing-Edge Serrations," *Journal of Fluid Mechanics*, Vol. 706, 2012, p. 295–322.

[47]Sanjosé, M., Moreau, S., Lyu, B., and Ayton, L. J., "Analytical, Numerical and Experimental Investigation of Trailing-Edge Noise Reduction on a Controlled Diffusion Airfoil with Serrations," AIAA 2019-2450, Proceedings of the 25th AIAA/CEAS Aeroacoustics Conference, Delft, The Netherlands, 20-23 May, 2019.

[48]Drela, M., *XFOIL: An Analysis and Design System for Low Reynolds Number Airfoils*, Vol. 54, Springer, 1989. Mueller T.J. (eds) Low Reynolds Number Aerodynamics.

[49]Peters, D., Boyd, D., and He, C., "Finite-State Induced-Flow Model for Rotors in Hover and Forward Flight," *Journal of the American Helicopter Society*, Vol. 34 (5), 1989, pp. 5–17, DOI: 10.4050/JAHS.34.5.

[50]Johnson, W., *Helicopter Theory*, Dover Publication, 1994.

[51]Li, S., and Lee, S., "Prediction of Urban Air Mobility Multirotor VTOL Broadband Noise Using UCD-QuietFly," *Journal of the American Helicopter Society*, **66**, 032004(2021), DOI: 10.4050/JAHS.66.032004.

[52]Amiet, R., "Noise Due to Turbulent Flow Past a Trailing Edge," *Journal of Sound and Vibration*, Vol. 47 (3), 1976, pp. 387–393.

[53]Roger, M., and Moreau, S., "Back-Scattering Correction and Further Extensions of Amiet's Trailing-Edge Noise Model. Part 1: Theory," *Journal of Sound and Vibration*, Vol. 286, 2005, pp. 477 – 506.

[54]Moreau, S., and Roger, M., "Back-Scattering Correction and Further Extensions of Amiet's Trailing-Edge Noise Model. Part II: Application," *Journal of Sound and Vibration*, Vol. 323, 2009, pp. 397–425.

[55]Li, S., and Lee, S., "Prediction of Rotorcraft Broadband Trailing-Edge Noise and Parameter Sensitivity Study," *Journal of the American Helicopter Society*, **65**, 042006(2020), DOI: 10.4050/JAHS.65.042006.

[56]Schlinker, R., and Amiet, R., "Helicopter Rotor Trailing Edge Noise," , 1981. NASA RP 3470.

[57]Lighthill, M., "On Sound Generated Aerodynamically I. General Theory," *Proceedings of the Royal Society*, Vol. A211, 1952, pp. 564–587.

[58]Lee, S., and Shum, J., "Prediction of Airfoil Trailing-Edge Noise Using Empirical Wall-Pressure Spectrum Models," *AIAA Journal*, Vol. 57 (3), 2019, pp. 888–897.

[59]Corcos, G. M., "The Structure of the Turbulent Pressure Field in Boundary-Layer Flows," *Journal of Fluid Mechanics*, Vol. 18 (3), 1964, p. 353–378.

[60]Brooks, T., and Hodgson, T., "Trailing Edge Noise Prediction from Measured Surface Pressures," *Journal of Sound and Vibration*, Vol. 78 (1), 1981, pp. 69–117.

[61]Li, S., and Lee, S., "Predictions and Validations of Small-Scale Rotor Noise Using UCD-QuietFly," Proceedings of the Vertical Flight Society 2022 Transformative Vertical Flight - Aeromechanics for Advanced Vertical Flight Technical Meeting, San Jose, CA, January 25-27, 2022.

[62]Kholodov, P., and Moreau, S., "Optimization of Trailing-Edge Serrations with and without Slits for Broadband Noise Reduction," *Journal of Sound Vibration*, Vol. 490, 2021, p. 115736.

[63]Li, S., "Development of Rotorcraft Forward Flight Analysis Code Using the Finite-State Dynamic Inflow Model," Master's thesis, University of California Davis, August 2020.

[64]Li, S., and Lee, S., "A Machine Learning-Based Fast Prediction of Rotorcraft Broadband Noise," AIAA 2020-2588, Proceedings of the 2020 AIAA Aviation Forum, Virtual Event, June 15-19, 2020.

[65]Jung, Y., Baeder, J., and He, C., "Investigation of Empirical Rotor Broadband Prediction using CFD Boundary Layer Parameters Extraction," Proceedings of the Vertical Flight Society 77th Annual Forum, Virtual Event, May 11-13, 2021.

[66]Won, J., Trembois, N., and Lee, S., "Towards Accurate Broadband Noise Predictions Using CFD," Proceedings of the Vertical Flight Society 79th Annual Forum, West Palm Beach, FL, May 16-18, 2023.

[67]Gill, H., and Lee, S., "Effect of 2D Ice Accretion on Turbulent Boundary Layer and Trailing-edge Noise," *International Journal of Aeroacoustics*, Vol. 21 (3-4), 2022, pp. 260–285.

[68]Lee, S., "Application of a Third Approximation to Glauert's Equations with Swirl to a Blade Element Momentum Theory," Proceedings of the AHS 73rd Annual Forum, Fort Worth, TX, May 9–11, 2017.

[69]Leon, C., Ragni, D., Probsting, S., Scarano, F., and Madsen, J., "Flow Topology and Acoustic Emissions of Trailing Edge Serrations at Incidence," *Experiments in Fluids*, Vol. 57 (91), 2016, pp. 1–17.

[70]Chong, T. P., and Vathylakis, A., "On the Aeroacoustic and Flow Structures Developed on a Flat Plate with a Serrated Sawtooth Trailing Edge," *Journal of Sound and Vibration*, Vol. 354, 2015, pp. 65–90.

[71]Gruber, M., Joseph, P., and Chong, T. P., "Experimental Investigation of Airfoil Self Noise and Turbulent Wake Reduction by the Use of Trailing Edge Serrations," AIAA 2010-3803, Proceedings of the 16th AIAA/CEAS Aeroacoustics Conference, Stockholm, Sweden, June 7-9, 2010.

[72]Johnson, W., and Silva, C., "NASA Concept Vehicles and the Engineering of Advanced Air Mobility Aircraft," *The Aeronautical Journal*, Vol. 126 (1295), 2022, p. 59–91.

[73]Kottapalli, S., and Silva, C., "Prediction of Quadrotor Acoustics Using RVLT Toolchain," Proceedings of the VFS Aeromechanics for Advanced Vertical Flight Technical Meeting, San Jose, CA, 25-27, 2022.

[74]Begault, D., "Ambient Noise Measurement for UAM Metric Analysis and Research," Acoustics and Urban Air Mobility Technical Working Group Meeting, Hampton, VA, April 09-11, 2019.

[75]Sanjose, M., Meon, C., Moreau, S., Idier, A., and Laffay, P., "Direct Numerical Simulation of Acoustic Reduction Using Serrated Trailing-Edge on an Isolated Airfoil," AIAA 2014-2324, Proceedings of the 20th AIAA/CEAS Aeroacoustics Conference, Atlanta, GA, June 16-20, 2014.

List of Figures

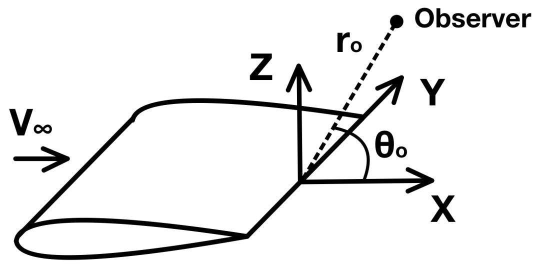

Fig. 1: Observer distance and angle in the blade local coordinates.

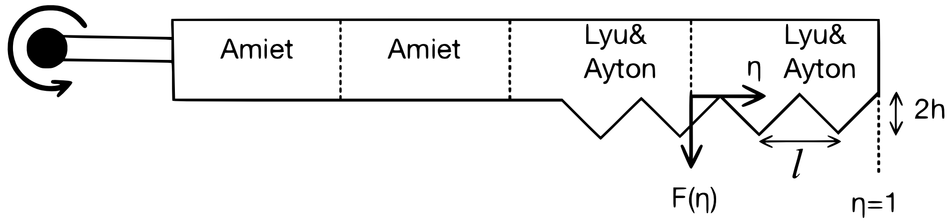

Fig. 2: Serrated rotor blade geometry.

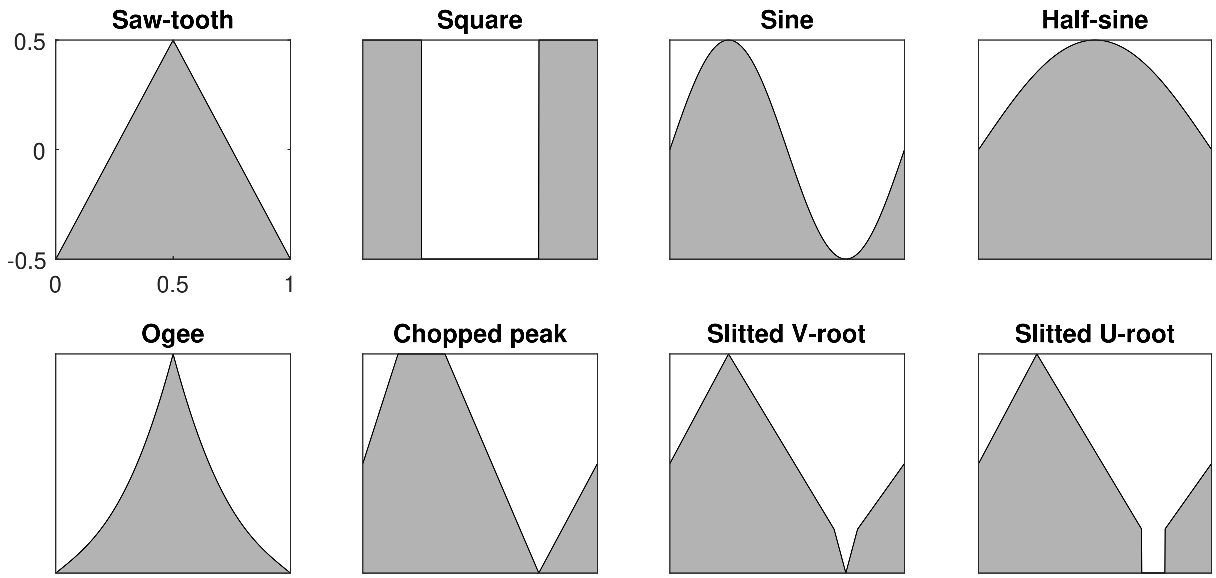

Fig. 3: Trailing-edge serrated geometries. The $\eta - F$ serration coordinate has the origin at the lower-left corner with the serration wavelength of l.

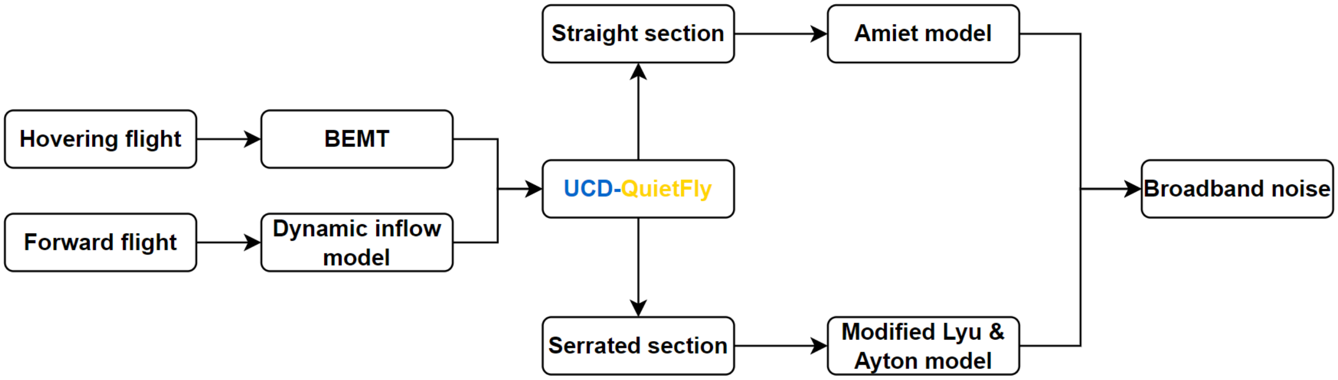

Fig. 4: Flowchart of Serrated Rotor Broadband Noise Prediction.

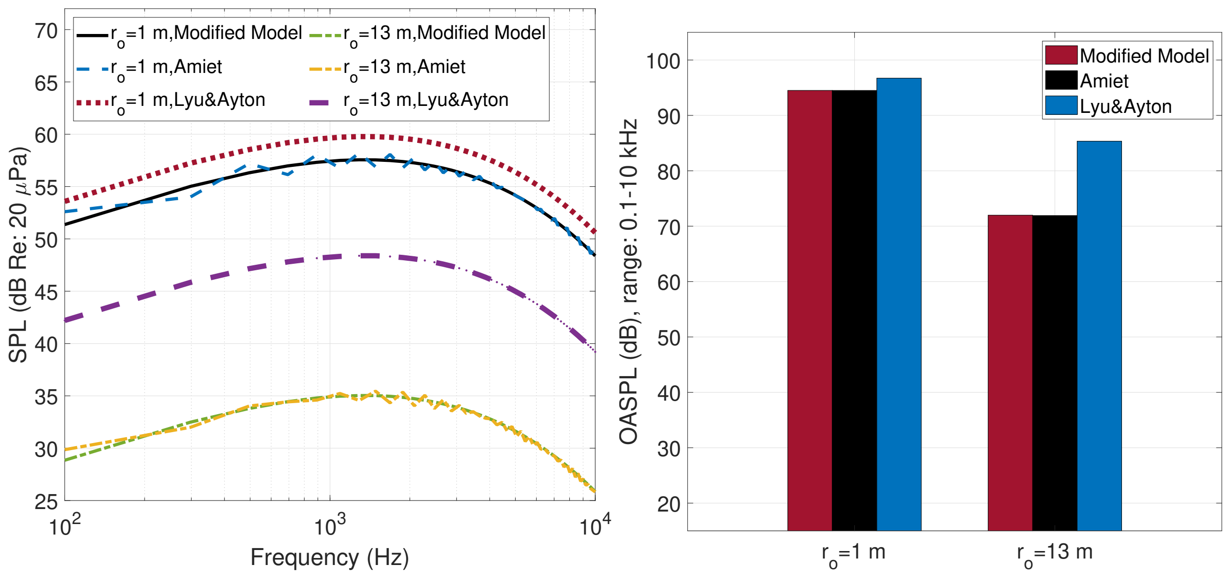

(a) (b)

Fig. 5: Comparison of Amiet's model and the modified Lyu and Ayton's model on a straight wing section at different observer distances and θ_o = 90 deg, for (a) frequency spectrum, and (b) overall sound pressure level.

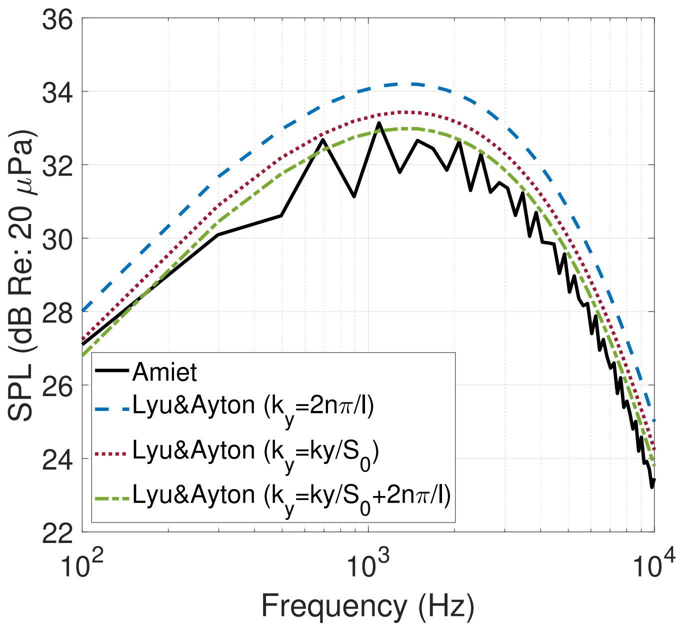

Fig. 6: Effect of the spanwise wavenumber in Lyu & Ayton's model on a straight wing section. r_o = 14.35 m, and θ_o = 85.6 deg.

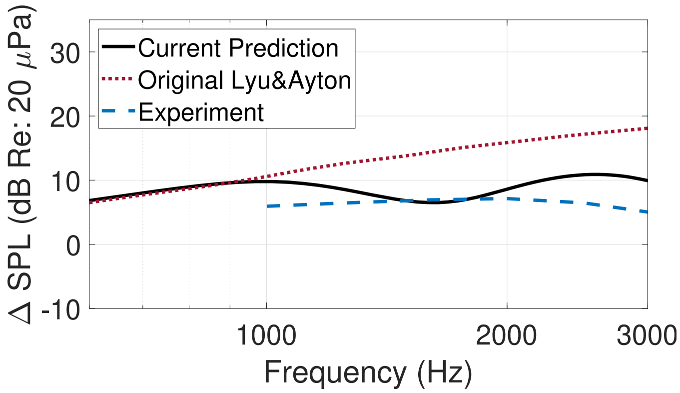

Fig. 7: Noise reduction validation of the serrated trailing-edge noise model on the wing section. The serration shape is sawtooth, $2h$ = 0.04 m, l = 0.02 m, r_o = 1.0548 m, and θ_o = 90 deg. Original Lyu and Ayton prediction is given in Ref. 44. Experiment data is given in Ref. 69.

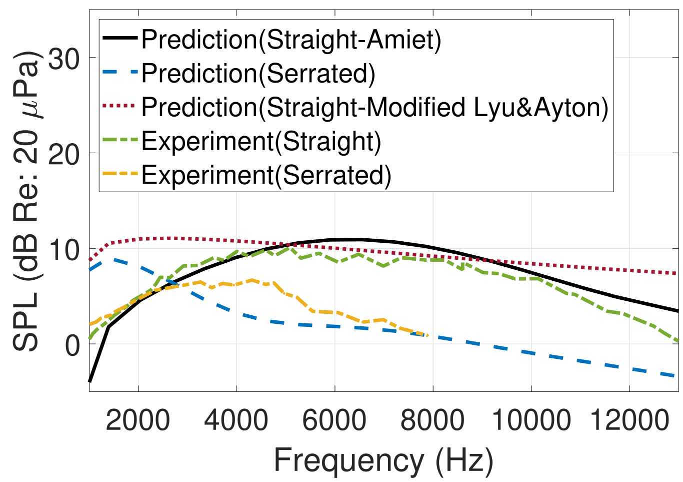

Fig. 8: Validation of UCD-QuietFly on the serrated APC drone rotor. r_o = 1.65 m, and ϕ_o = 90 deg. Experiment data is given in Ref. 35, with broadband components extracted.

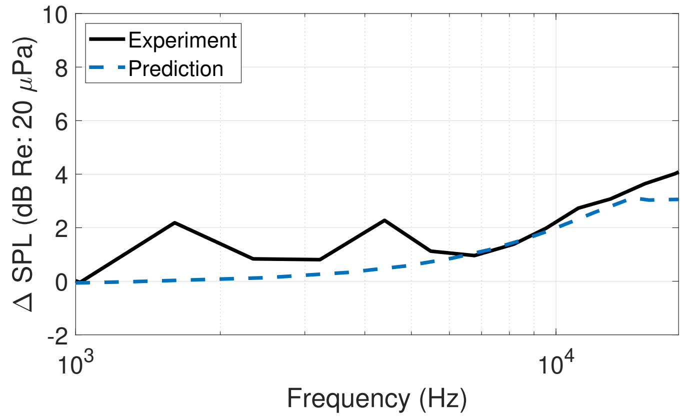

Fig. 9: Validation of UCD-QuietFly on the serrated eHANG drone rotor in forward flight. $r_o = 1.49$ m, and $\phi_o =$ -56.31 deg. Experiment data is given in Ref. 36, with broadband components extracted.

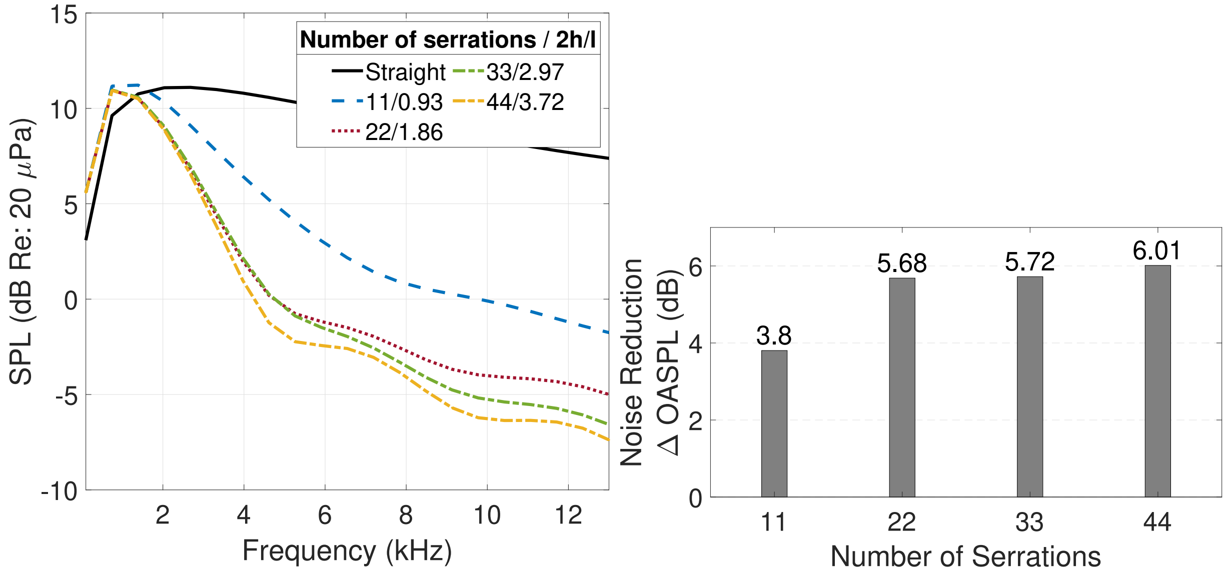

(a)

(b)

Fig. 10: The effect of the number of serrations on rotor broadband noise: (a) sound pressure level spectrum and (b) noise reduction compared to the straight-blade rotor. r_o = 150 m, and ϕ_o = -90 deg.

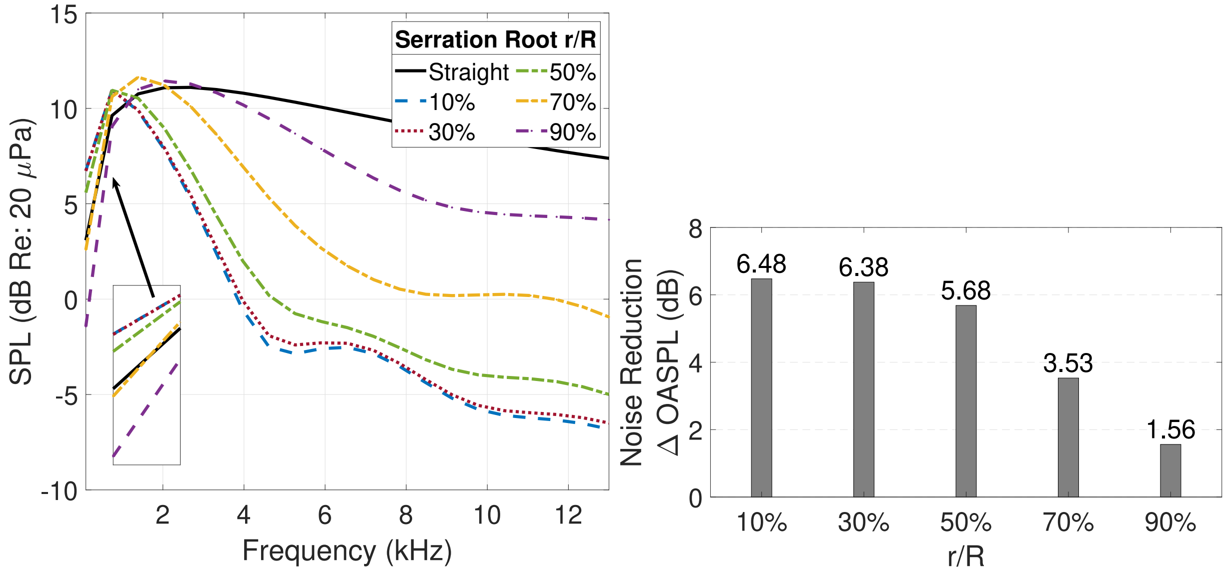

(a) (b)

Fig. 11: The effect of starting radial locations of the serrations on rotor broadband noise: (a) sound pressure level spectrum and (b) overall sound pressure level reduction compared to the straight-blade rotor.

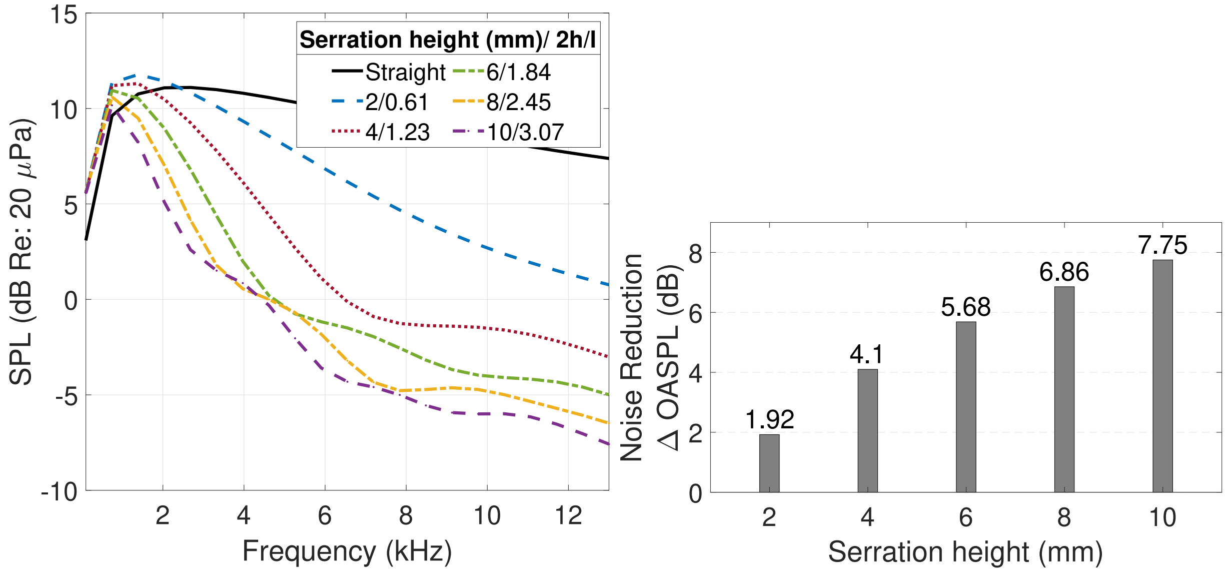

(a) (b)

Fig. 12: The effect of serration heights on rotor broadband noise: (a) sound pressure level spectrum and (b) overall sound pressure level reduction compared to the straight-blade rotor.

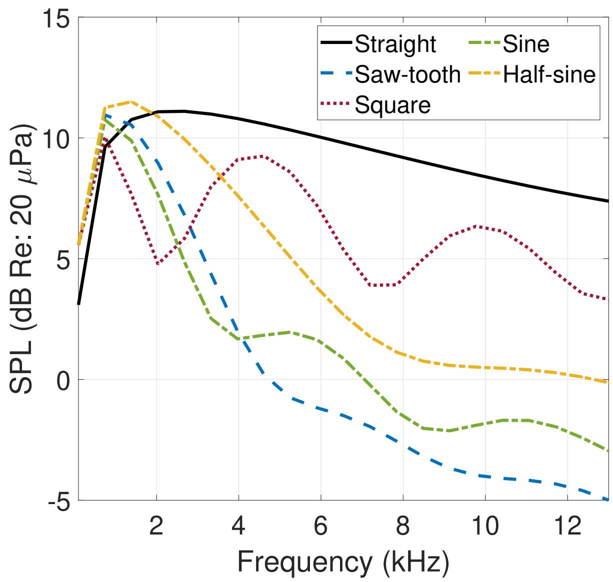

(a)

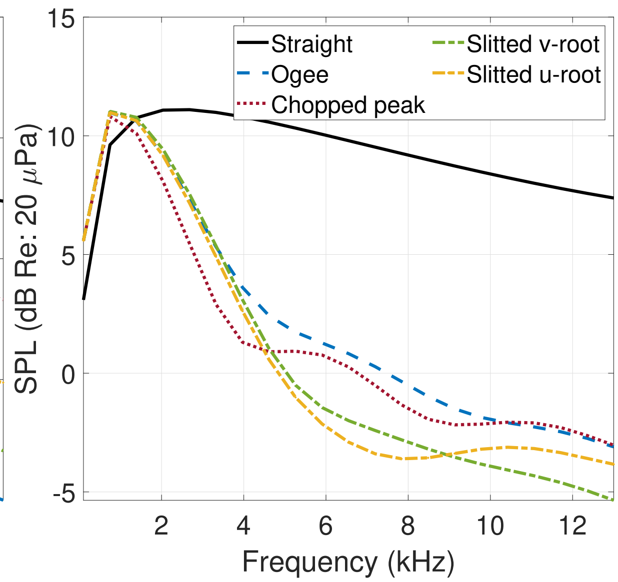

(b)

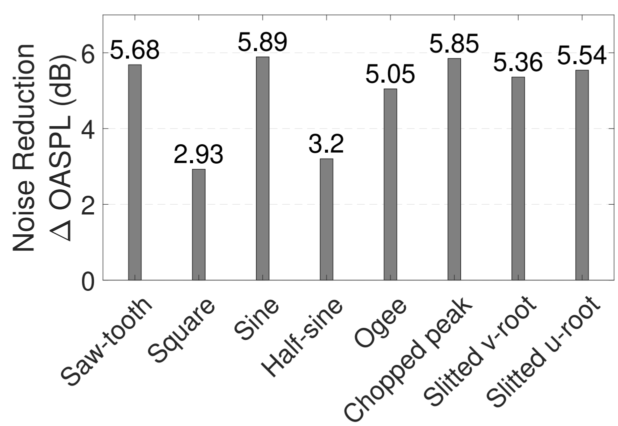

(c)

Fig. 13: The effect of serration shapes, with the same wavelength and height, on rotor broadband noise: (a) (b) sound pressure level spectrum of the shapes in Eq. (16), and (c) overall sound pressure level reduction compared to the straight-blade rotor.

Fig. 14: Conceptual design of an electric quadrotor (Ref. 20).

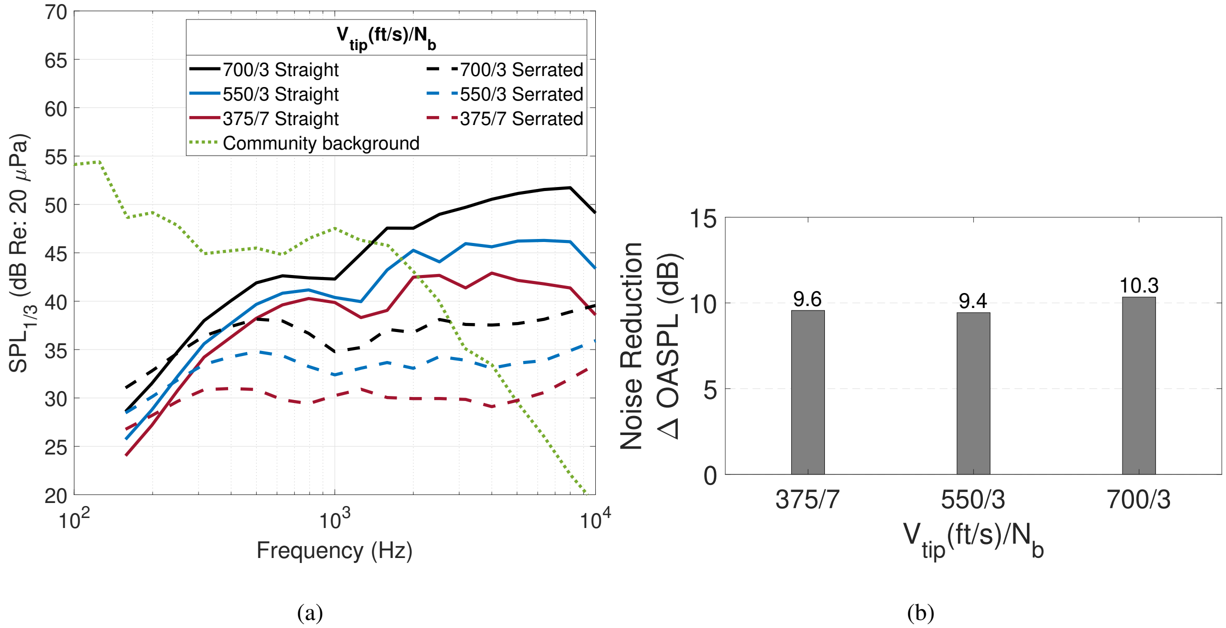

Fig. 15: Effects of using serrated blades on broadband noise of an eVTOL quadrotor with various design tip speeds and numbers of blades. The observer is located at 492 ft (150 m) directly underneath the vehicle. The serration height is $2h$ = 0.0702 m and the serration wavelength is l = 0.0351 m. The community background noise is given in (Ref. 74): (a) sound pressure level spectrum and (b) overall sound pressure level reduction compared with the straight-blade rotor.

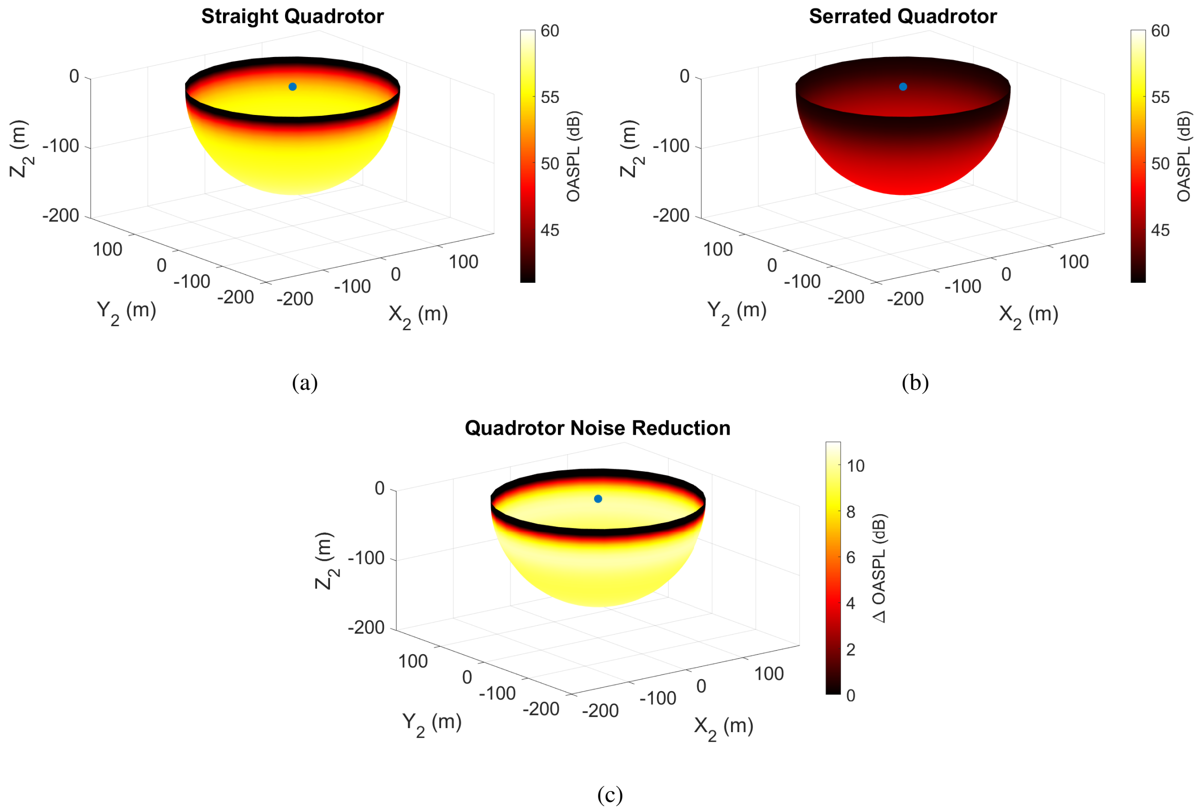

Fig. 16: Hemispheric directivity of broadband noise OASPL (0.1-13 kHz) of the UAM eVTOL quadrotor with three blades and the tip speed of 700 ft/s: (a) straight blade, (b) serrated blade, and (c) noise reduction.

Fig. 17: Conceptual design of a quiet helicopter (Ref. 18).

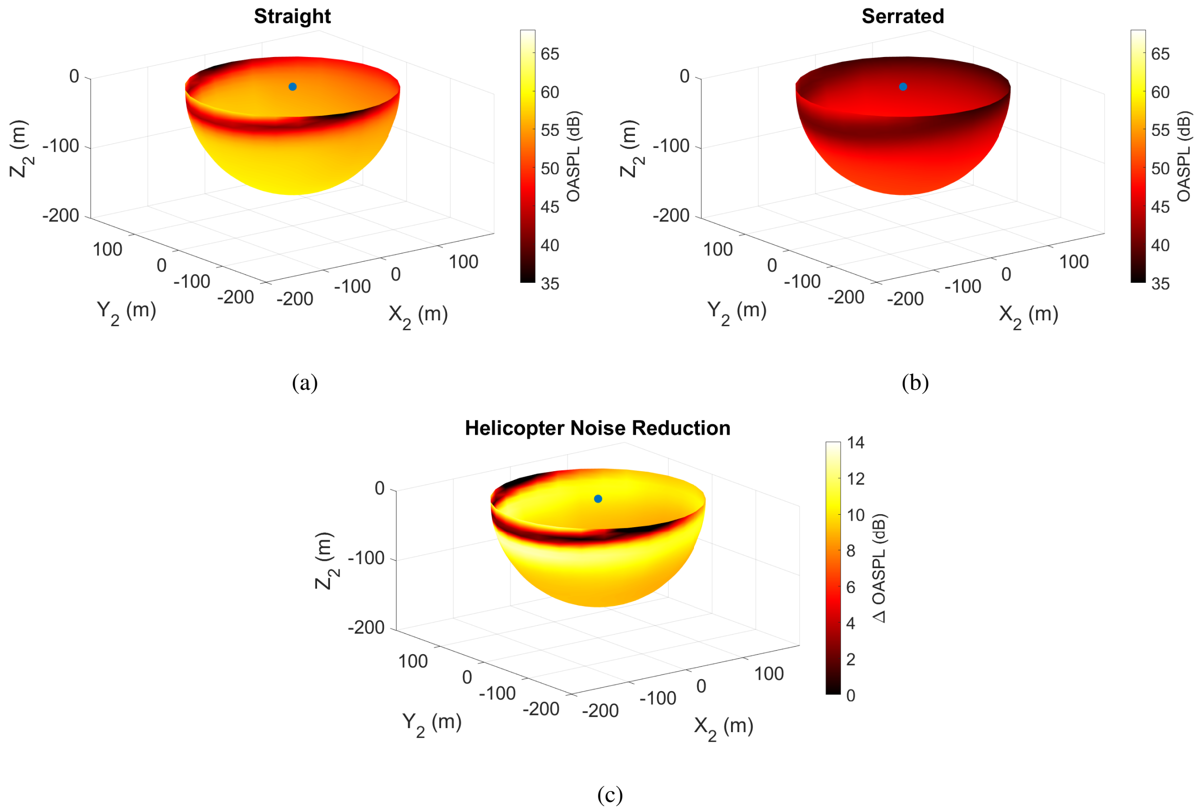

Fig. 18: Hemispheric directivity of broadband noise OASPL (0.1-13 kHz) of a quiet helicopter design in forward flight with three blades and the tip speed of 700 ft/s: (a) straight blade, (b) serrated blade, and (c) noise reduction.

List of Tables

Table 1: Parameters for Validation of Trailing-Edge Noise from a Wing Section

Parameters	Verification (Fig. 5(a))	Verification (Fig. 6)	Validation (Fig. 7)
Airfoil	NACA 0012	NACA 0012	NACA 0018
TE geometry	straight	straight	serrated
V_0 (m/s)	241	241	34
α (deg)	1.8	1.8	0.0
c (m)	0.2	0.2	0.2
Δr (m)	0.15	0.15	0.4
r_o (m)	1 & 13	14.35	1.0548
θ_o (deg)	90	85.6	90
y (m)	0	6	0

Table 2: Hovering Rotor Validation Parameters

Parameters	APC 11X4.7	eHANG Ghost 3.0	Quadrotor	Quiet helicopter
R (m)	0.14	0.13	2.808	5.17
N_b	2	2	3/3/7	3
RPM	3000	7200	726/570/389	394
Airfoil	E63(hub)/ClarkY(tip)	A18	VR-12/SSC-A09	VR-12/SSC-A09
ϕ_o (deg)	90	-56.31	-90	-90
μ (deg)	0	0	0	0.246
r_o (m)	1.65	1.49	150	150
Shape	Saw-tooth	Saw-tooth	Saw-tooth	Saw-tooth
$2h$ (m)	0.006	0.00326	0.0702	0.258
l (m)	0.00322	0.00652	0.0351	0.129
serration r/R range	0.5-1.0	0.2-1.0	0.5-1.0	0.5-1.0